Article

Synthesis of Polystyrene@TiO$_2$ Core–Shell Particles and Their Photocatalytic Activity for the Decomposition of Methylene Blue

Naoki Toyama [1,*] , **Tatsuya Takahashi [2]** , **Norifumi Terui [2]** and **Shigeki Furukawa [1]**

[1] Department of Sustainable Engineering, College of Industrial Technology, Nihon University, 1-2-1, Izuni-cho, Narashino 275-8575, Chiba, Japan; furukawa.shigeki@nihon-u.ac.jp

[2] Department of Engineering for Future Innovation, National Institute of Technology, Ichinoseki College, Takanashi, Hagisho, Ichinoseki 021-8511, Iwate, Japan; t.tatsuya21806@gmail.com (T.T.); terui@ichinoseki.ac.jp (N.T.)

[*] Correspondence: toyama.naoki@nihon-u.ac.jp

Abstract: In this study, we investigated the preparation conditions of polystyrene (PS)@TiO$_2$ core–shell particles and their photocatalytic activity during the decomposition of methylene blue (MB). TiO$_2$ shells were formed on the surfaces of PS particles using the sol–gel method. Homogeneous PS@TiO$_2$ core–shell particles were obtained using an aqueous NH$_3$ solution as the promoter of the sol–gel reaction and stirred at room temperature. This investigation revealed that the temperature and amount of the sol–gel reaction promoter influenced the morphology of the PS@TiO$_2$ core–shell particles. The TiO$_2$ shell thickness of the PS@TiO$_2$ core–shell particles was approximately 5 nm, as observed using transmission electron microscopy. Additionally, Ti elements were detected on the surfaces of the PS@TiO$_2$ core–shell particles using energy-dispersive X-ray spectroscopy analysis. The PS@TiO$_2$ core–shell particles were used in MB decomposition to evaluate their photocatalytic activities. For comparison, we utilized commercial P25 and TiO$_2$ particles prepared using the sol–gel method. The results showed that the PS@TiO$_2$ core–shell particles exhibited higher activity than that of the compared samples.

Keywords: titania; polystyrene; core–shell; methylene blue; photocatalytic activity

1. Introduction

As environmental pollution continues to worsen, technologies and materials that mitigate this issue have become widely researched topics [1,2]. Organic dyes primarily released from industrial plants are among such pollutants that form part of effluents in various water bodies [3,4]. Dyes such as methylene blue (MB) are toxic and nonbiodegradable, and they remain in the water for long periods of time [5]. Therefore, developing methods for removing dyes from water bodies is crucial.

Many approaches have been reported for dye removal, such as flocculation, chemical oxidation, membrane filtration, chemical coagulation, photochemical degradation, and biological degradation [4–6]. Notably, photocatalysis is an effective method for dye degradation because of its advantages, such as its eco-friendliness, high efficiency, low cost, and reusability [7,8]. Recently, hydrogen evolution was promoted in the presence of photocatalysts such as metal compound/g-C$_3$N$_4$ systems and flower-like carbon quantum dots/BiOBr composites [9–13].

Titanium dioxide (TiO$_2$) is well known for being an excellent photocatalyst. This oxide has attracted attention for use in pollutant removal because it offers high conversion efficiency, good chemical stability, and low cost [14–16]. The sol–gel reaction has been reported as a synthetic method for generating TiO$_2$ particles [17,18]. In general, TiO$_2$ particles with a small particle size can efficiently act as a photocatalyst; however, these tend

to agglomerate due to their high energy and reduce the number of available active sites [19]. To solve this problem, TiO_2 particles have been immobilized on polymer substrates such as polymers, including polyethlene [20,21] and poly (dimethylsiloxane) beads, [22] and so on [23]. Moreover, it is difficult to obtain TiO_2 particles with uniform size due to the fast sol–gel reaction rates exhibited by Ti precursors [24,25]. Therefore, the challenge is to immobilize TiO_2 particles uniformly on the surfaces of substrates. Additionally, many complex processes are required in order to obtain substrate-supported TiO_2 particles due their long synthesis time [26–28]. We propose a facile method for the immobilization of TiO_2 particles on the surfaces of polystyrene (PS) particles.

Monodisperse PS particles with a positive charge were prepared using emulsifier-free emulsion polymerization using 2′2-azodiisobutyramidine dihydrochloride as the initiator and poly (vinylpyrrolidone) as the stabilizer [29–31]. Previous studies found that SiO_2-Al_2O_3 nanoparticles could be collected on the surfaces of PS particles. In this method, the SiO_2-Al_2O_3 nanoparticles were prepared using the sol–gel method, and the nanoparticles with negative charges were attracted to the surfaces of the PS particles because of their positive charges, thus forming SiO_2-Al_2O_3 shells [32]. With this knowledge in mind, we attempted to collect TiO_2 particles on the surfaces of PS particles using this simple method.

Herein, we report PS@TiO_2 core–shell particles synthesized using the sol–gel method. In this method, TiO_2 shells were formed on the surfaces of PS particles. Homogeneous spherical particles were obtained by adjusting the reaction temperature and amount of the promoter aqueous NH_3 solution. A schematic illustration of the synthesis of the PS@TiO_2 core–shell particles is shown in Figure 1. Experimental observations confirmed that the diameters of PS@TiO_2 core–shell particles were approximately 220 nm. Furthermore, TiO_2 was confirmed to be present on the surfaces of the PS@TiO_2 core–shell particles. The photocatalytic activity of the PS@TiO_2 core–shell particles was evaluated using MB decomposition. The PS@TiO_2 core–shell particles showed better performance than that of the commercial P25.
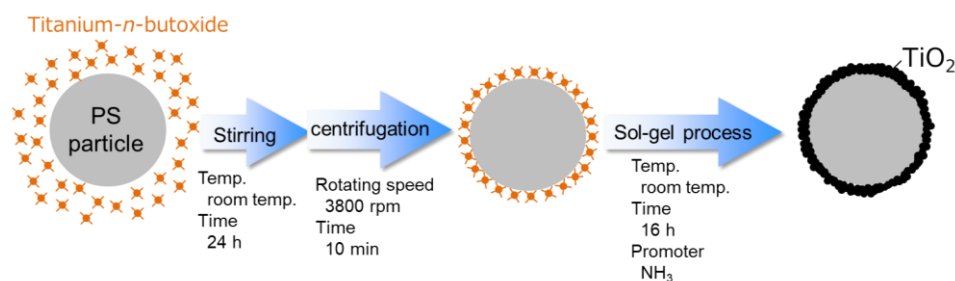

Figure 1. Schematic illustration of the formation process of PS@TiO_2 core–shell particles.

2. Results and Discussion

First, we investigated the influence of preparation conditions such as the preparation temperature and amount of aqueous NH_3 solution on the morphology of PS@TiO_2 core–shell particles. Figure 2a–c show scanning electron microscopy (SEM) images of PS@TiO_2 core–shell particles prepared at various preparation temperatures and with varying amounts of aqueous NH_3 solution. Uniform spherical particles were prepared using 300 µL of aqueous NH_3 solution at room temperature (Figure 2a), whereas spherical particles and particles with irregular shapes were prepared using 300 µL of aqueous NH_3 solution at 323 K (Figure 2b). Meanwhile, the rough layers, including spherical particles on the surface, were observed in SEM images of Figure 2c when prepared using 1000 µL of aqueous NH_3 solution at room temperature. Using this process, the TiO_2 nanoparticles prepared via the sol–gel reaction were collected on the surfaces of PS particles. Reportedly, the sol–gel reaction rate enhances higher temperatures and increases the amounts of promoters such as NH_3 [33]. Consistent with the above reports, a faster sol–gel reaction rate promoted TiO_2 particle growth, leading to the formation of particles with irregular shapes and rough layers, as shown in Figure 2b,c. Moreover, we confirmed the presence of TiO_2

on the surfaces of uniform PS@TiO$_2$ core–shell particles prepared using 300 µL of aqueous NH$_3$ solution at room temperature through energy-dispersive X-ray spectroscopy (EDX) measurements. Figure 3 shows elemental mapping images of O, Ti, and C for the prepared PS@TiO$_2$ core–shell particles. O and Ti were observed in the overall images, and the ratio of O:Ti was approximately 1:1. Additionally, the areas of C elemental mapping overlapped the areas of Ti and O elemental mapping. This result suggests that very thin TiO$_2$ shells can be formed on the surfaces of PS particles. Meanwhile, we measured the specific surface area of the PS@TiO$_2$ core–shell particles using the Brunauer–Emmett–Teller (BET) method. The results showed that the specific surface area of the PS@TiO$_2$ core–shell particles was 125 m^2 g^{-1}.
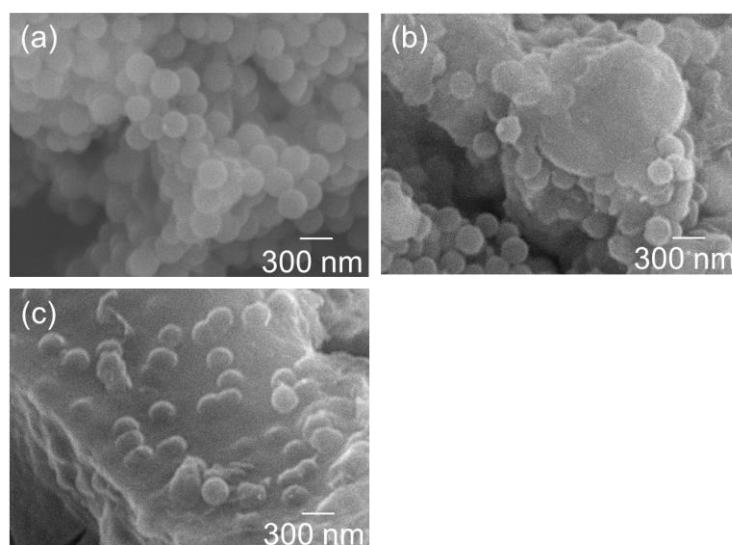

Figure 2. SEM images of PS@TiO$_2$ core–shell particles prepared at (**a**) room temperature, (**b**) 323 K using 300 µL of aqueous NH$_3$ solution, and (**c**) room temperature using 1000 µL of aqueous NH$_3$ solution.
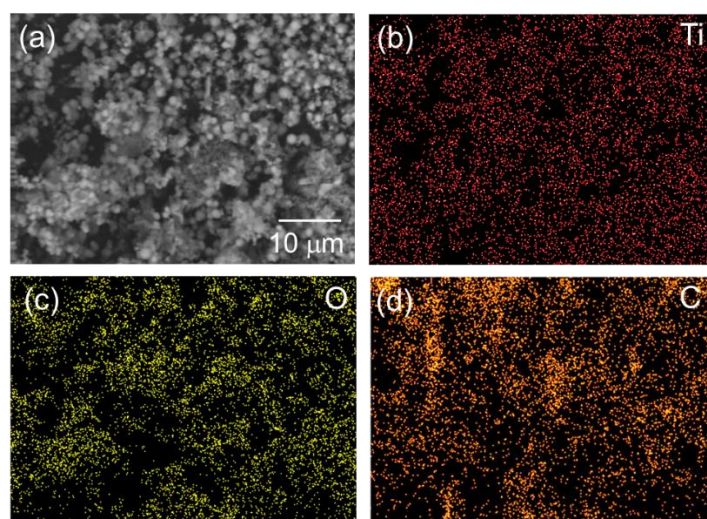

Figure 3. SEM/EDX images of (**a**) PS@TiO$_2$ core–shell particles and element mappings of (**b**) Ti, (**c**) O, and (**d**) C.

Next, the morphology of PS@TiO$_2$ core–shell particles were observed in detail using transmission electron microscopy (TEM). For comparison, we used TiO$_2$ particles prepared using sol–gel reactions and commercial P25. Figure 4a shows a TEM image of PS particles. In this image, the diameters of the PS particles are approximately 280 nm. Figure 4b,c show TEM images of the PS@TiO$_2$ core–shell particles. The obtained images show that

the diameters of the spherical particles were approximately 290 nm. The presence of the TiO_2 shell was confirmed by the different contrasts between core and shell. As shown in Figure 4a–c, the shell thickness of the PS@TiO_2 core–shell particles could be ~5 nm. This result is also consistent with the results of the SEM/energy-dispersive X-ray spectroscopy (EDX) element mapping images, which show the detection of C (Figure 3). Meanwhile, the presence of prepared TiO_2 particles and P25 was also confirmed using the TEM images. In these results, the prepared TiO_2 is presented in random shapes (Figure 4d), whereas crystal particles with diameters of 20–50 nm are observed in the TEM image of P25 (Figure 4e).
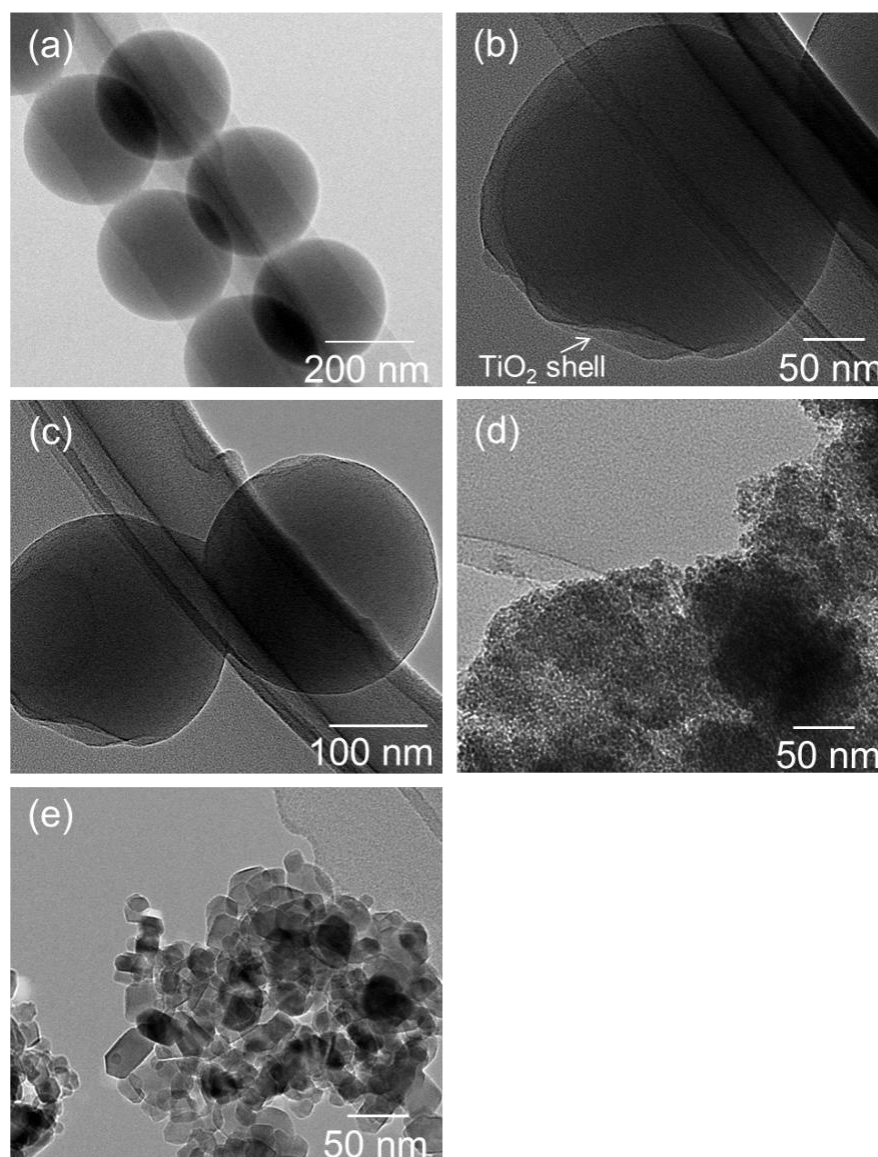

Figure 4. TEM images of (**a**) PS particles, (**b**,**c**) PS@TiO_2 core–shell particles, (**d**) prepared TiO_2, and (**e**) commercial P25.

The crystallinity of the samples was measured using powder X-ray diffraction (XRD). Figure 5 shows the XRD patterns of the PS@TiO_2 core–shell particles, the prepared TiO_2, and the commercial P25. The PS@TiO_2 core–shell particles showed a broad diffraction peak, whereas the prepared TiO_2 showed no peak, indicating that both samples were composed of an amorphous phase. Meanwhile, the commercial P25 showed sharp peaks, indicating that it was composed of rutile and anatase phases [34].
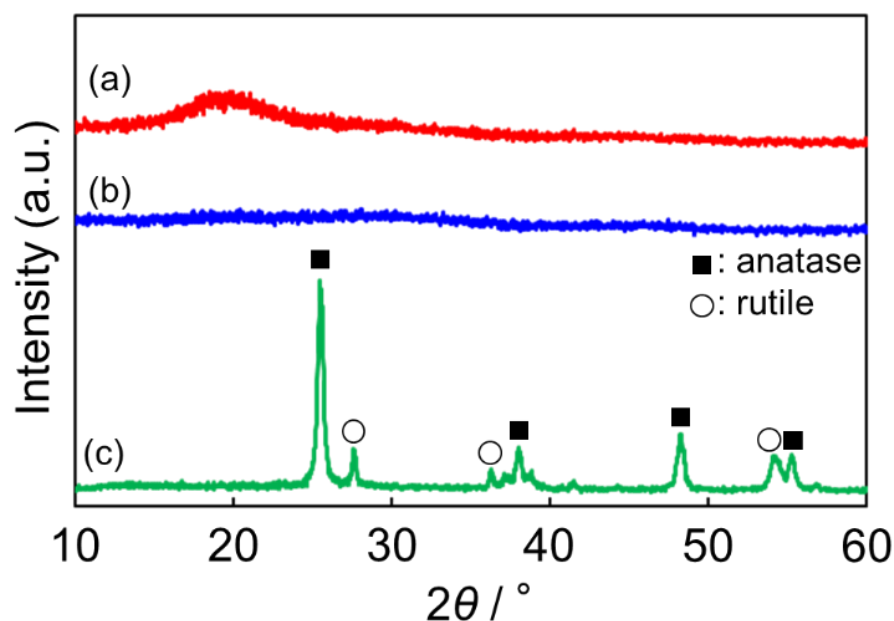
Figure 5. XRD patterns of (**a**) the PS@TiO$_2$ core–shell particles, (**b**) the prepared TiO$_2$, and (**c**) the commercial P25.

Finally, the photocatalytic activities of the PS@TiO$_2$ core–shell particles, the prepared TiO$_2$, and the commercial P25 were evaluated through MB decomposition. The main peak of MB was observed at 664 nm. The UV visible (UV-Vis) absorption spectra of the PS@TiO$_2$ core–shell particles, the prepared TiO$_2$, the commercial P25, and the PS particles monitored at different times are shown in Figure 6a–d. As seen in these results, the intensity of the absorption peak gradually decreased with the reaction time in the presence of the PS@TiO$_2$ core–shell particles, the prepared TiO$_2$, and the commercial P25. However, the intensity of the absorption peak was not changed in the presence of the PS particles. Figure 6e shows the reaction time dependence of MB decomposition in the presence of these samples with UV irradiation. The relative intensity of the absorbance at 664 nm was used to calculate the value of C/C_0, where C_0 and C are the MB concentrations of the aqueous MB solution at the beginning and reaction time, respectively. In the presence of the PS@TiO$_2$ core–shell particles and the prepared TiO$_2$, 84% and 38% of MB degraded within 3 min. Meanwhile, 84% and 60% of MB degraded within 24 min, indicating that both samples did not promote MB decomposition after 4 min. In the case of the commercial P25, the intensity of the main peak gradually decreased with the increase in reaction time, and 58% of MB degraded after 24 min. On the other hand, the PS particles showed no activity. These results indicate that the PS@TiO$_2$ core–shell particles demonstrated a faster reaction rate than those of the prepared TiO$_2$ and the commercial P25.

The PS@TiO$_2$ core–shell particles were used in MB decomposition with and without UV irradiation to evaluate their photocatalytic activity. Figure 7a shows the UV-Vis absorption spectra of the reaction solutions with the PS@TiO$_2$ core–shell particles without UV irradiation. The intensity of the absorption peak at 664 nm was unchanged without UV irradiation. Figure 7b shows the reaction time dependence in the presence of the PS@TiO$_2$ core–shell particles with and without UV irradiation. With UV irradiation, 87% of MB degraded after 24 min, as described in the above results, whereas without UV irradiation, MB decomposition was not promoted.
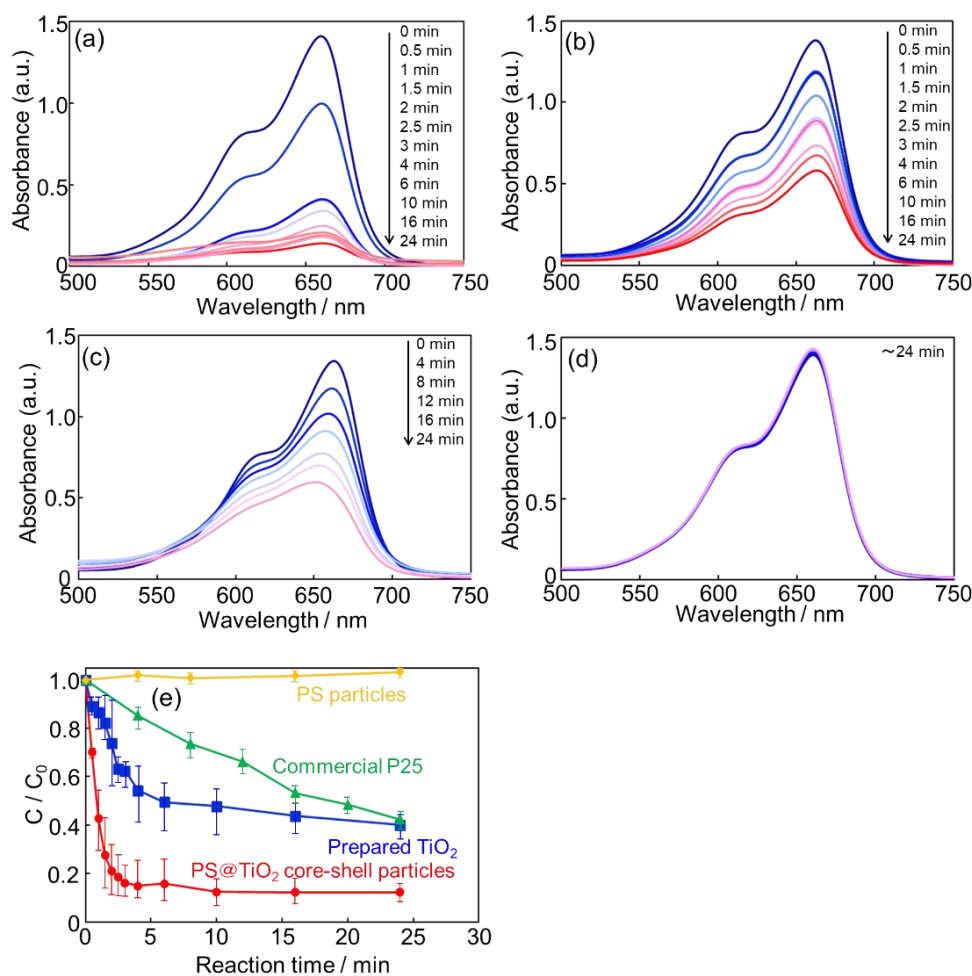
Figure 6. UV-Vis absorption spectra of the reaction solutions with (**a**) PS@TiO$_2$ core–shell particles, (**b**) prepared TiO$_2$, (**c**) commercial P25, and (**d**) PS particles. (**e**) Relationship between C/C_0 and the reaction time for MB decomposition.
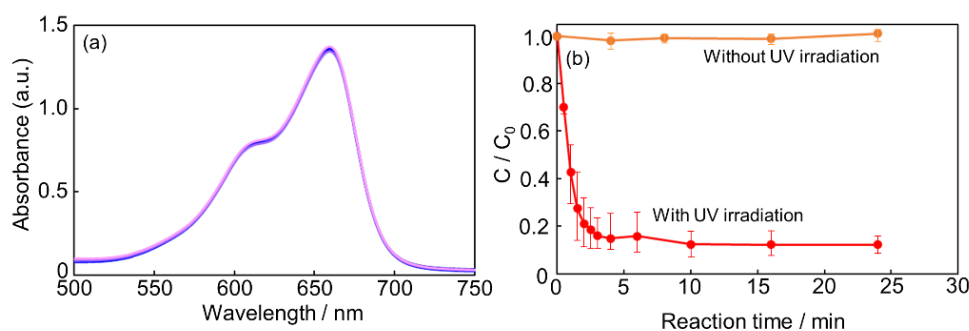

Figure 7. UV-Vis absorption spectra of the reaction solutions with (**a**) PS@TiO$_2$ core–shell particles without UV irradiation. (**b**) Relationship between C/C_0 and the reaction time for MB decomposition in the presence of the PS@TiO$_2$ core–shell particles with and without UV irradiation.

Herein, we discussed the differences in the photocatalytic activities of the PS@TiO$_2$ core–shell particles, the prepared TiO$_2$, and the commercial P25. First, we noted that PS@TiO$_2$ core–shell particles exhibited the highest MB decomposition activity. In this activity evaluation, the masses of the samples were equal, whereas the masses of TiO$_2$ were lower than the practical masses of the samples because PS@TiO$_2$ core–shell particles contained PS particles as the core. Nevertheless, the PS@TiO$_2$ core–shell particles exhibited the highest MB decomposition activity among all samples. This may have been because

TiO_2 shells with a shell thickness of about 5 nm were uniformly coated on surface of PS particles leading to efficient activity promotion. Therefore, the PS@TiO_2 core–shell particles, the prepared TiO_2, and the PS particles were investigated via photoluminescence (PL) measurements. Figure 8 shows the PL spectra of the PS@TiO_2 core–shell particles, the prepared TiO_2, and the PS particles. From this result, a broad peak was observed at around 390 nm for the PS@TiO_2 core–shell particles and the prepared TiO_2, while no peak was observed for the PS particles. In addition, the PS@TiO_2 core–shell particles exhibited a higher peak intensity than the prepared TiO_2. This peak was attributed to band-to-band transition [35]. Previous studies have reported that a peak was not observed for amorphous TiO_2 because of the lack of fluorescence [36], whereas for the TiO_2 with anatase crystalline phases, a peak was observed [35]. It may be that the TiO_2 shells on the surface of the PS@TiO_2 core–shell particles formed very tiny crystal particles with poor crystalline phases. The broad peaks observed at 20° in the XRD results may imply the existence of poor crystalline phases. In other reports, the peak intensity of the amorphous TiO_2 coating on the surface of ZnO particles increased compared with that of ZnO particles, indicating that the fine control of TiO_2 shell thickness on the surface of ZnO nanoparticles was very important for the enhancement of PL intensity [37]. Considering this, the crystallinity and thickness of the TiO_2 shell of PS@TiO_2 core–shell particles may play an important role in MB decomposition.
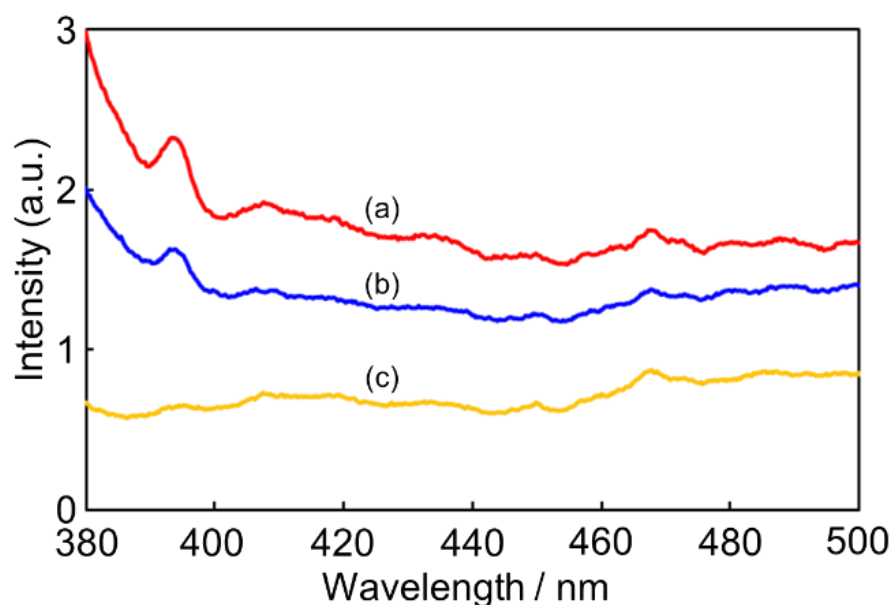

Figure 8. PL spectra of (a) PS@TiO_2 core–shell particles, (b) prepared TiO_2, and (c) PS particles.

Next, a comparison of the MB decomposition obtained in this study with those of other previously reported studies [38–42] is listed in Table 1. It was found that PS@TiO_2 core–shell particles show higher activity than most TiO_2-polymers and their related catalysts. However, the MB degradation rate per dosage of the PS@TiO_2 core–shell particles (0.379% $min^{-1}mg^{-1}$) was lower than that of TiO_2/graphene porous composites (0.64% $min^{-1}mg^{-1}$). This result might be ascribed to the different crystallinity of TiO_2. The TiO_2 shells of the PS@TiO_2 core–shell particles were probably amorphous phases, as shown in Figure 5a. On the other hand, the TiO_2 on the graphene porous composites was an anatase phase [42]. Indeed, the band gap of the amorphous TiO_2 is higher than that of the rutile and anatase TiO_2 [43]. Moreover, there may also be a difference in the mechanism of photocatalysis.

Table 1. Comparison of the MB decomposition of TiO_2-polymer photocatalysts in previous reports.

Samples	Light Source	MB Concentration	Dosage/mg	Degradation Rate/% min^{-1}	References
PS@TiO_2 core–shell particles	UV lamp (150 mW cm^{-2})	7 ppm (1.9 × 10^{-5} M)	10	3.67	This study
TiO_2 firm/ABS	Xenon lamp (300 W)	1.0 × 10^{-6} M	No data (3 × 3 cm)	0.67	38
PU/aTiO_2 Hybrid (10 wt%)	UV-A irradiation	10 ppm	No data	3.19	39
CAT-1 [*1]	Xenon lamp (300 W)	50 ppm	20	0.29	40
TiO_2/graphene porous composite	Xenon lamp (50 W)	10 ppm	1	0.64	41
TiO_2/porous carbon nanofibers	Xenon lamp (800 W)	10 ppm	50	1.88	42

[*1] CAT-1: TiO_2-MWCNT-C 1 hybrid aerogel.

In addition, we discussed the differences in reaction rates between the PS@TiO_2 core–shell particles and the commercial P25. The reaction rates of MB decomposition in the presence of the PS@TiO_2 core–shell particles and the commercial P25 from 0 to 4 min were 21.3% min^{-1} and 3.7% min^{-1}, respectively. Meanwhile, the reaction rates of MB decomposition from 4 to 24 min were 0.13% min^{-1} and 2.1% min^{-1}, respectively. The significantly faster reaction rate of the PS@TiO_2 core–shell particles might be related to the zeta potential of the samples. TiO_2 samples such as P25 reportedly have a negatively charged surface at a pH value of greater than 7 [44]. Meanwhile, the PS@TiO_2 core–shell particles have a negatively charged surface at a pH value of more than 4–5 [45,46]. Because the pH of the reaction solution was 6 in this study, the surface of the PS@TiO_2 core–shell particles was negatively charged, whereas the surface of the commercial P25 was positively charged. MB which have cationic ions were electrochemically attracted to the surface of the PS@TiO_2 core–shell particles, leading to an increase in the initial reaction rate. Meanwhile, the MB was electrochemically repelled from the surface of the commercial P25. The photocatalytic activity decreased after 4 min, probably because the rate of MB adsorption on the surface was faster than the rate of decomposition induced by the photocatalyst, and the MB covered the TiO_2 layer as it prevented the blocking of UV irradiation. In order to solve this problem, we suggest that TiO_2 hollow spheres are prepared via calcination of the PS@TiO_2 core–shell particles. The hollow spheres have high specific surface areas because of the void spaces, leading to an increase in contact frequency with the MB. We found that the PS particles can be decomposed via calcination at 723–873 K [47]. The crystallinity of the TiO_2 simultaneously grows during calcination. Based on this knowledge, we expect that TiO_2 hollow spheres with crystalline shells can efficiently act as photocatalysts.

3. Materials and Methods

3.1. Synthesis of PS@TiO_2 Core–Shell Particles and TiO_2 particles

PS particles were prepared with reference to a previous study [29]. The collected PS was washed with ethanol (10 mL, Kanto Chemical Co., Tokyo, Japan, >99.5%) via centrifugation at 3800 rpm for 10 min, twice. The final PS contents were dispersed in ethanol (15 mL). This PS suspension (10 g), titanium-*n*-butoxide (1000 μL, Kanto Chemical Co., >98.0%), and ethanol (40 mL) were stirred at room temperature for 24 h. The obtained suspension was centrifuged at 3800 rpm for 10 min and washed with ethanol to obtain the precursor of the PS@TiO_2 core–shell particles. The precursor was spread in ethanol (20 mL). After that, ethanol and an aqueous NH_3 solution (300 or 1000 μL, Kanto Chemical Co., 28.0–30.0% NH_3) were added to the precursor suspension, which was then stirred at room temperature or 323 K for 17 h. Then, the suspension was centrifuged at 3800 rpm for 10 min, and the collected white contents were dried in a desiccator overnight to obtain the PS@TiO_2 core–shell particles. For comparison, we utilized commercial P25 (Kanto Chemical Co.)

and TiO$_2$ particles prepared using the sol–gel method. The TiO$_2$ particles were prepared as follows: The titanium-*n*-butoxide (1000 μL), aqueous NH$_3$ solution (300 μL), and ethanol were stirred at room temperature for 1 h. After that, the white suspension was separated via filtration. The collected white powders were dried in a desiccator overnight to obtain the TiO$_2$ particles.

3.2. Characterization

The morphologies of the samples were observed via TEM (JEM 2010F, JEOL), operating at an accelerating voltage of 200 kV, and SEM (SU3500, JEOL), operating at an accelerating voltage of 15 kV. The chemical compositions and mapping images of the samples were determined using EDX spectroscopy. The specific surface areas of the samples were measured using N$_2$ sorption at 77 K using the BET method (Belsorp-mini, MicrotracBEL). The crystallites of the samples were determined using XRD (MultiFlex X-ray diffractometer, Rigaku) at 30 kV and 15 mA of CuKα radiation. PL measurement was performed to evaluate the samples using a fluorospectrophotometer with a Xe lamp light source (HITACHI, F-4500). The measurement excitation wavelength was set to 365 nm. All measurements of the sample were carried out at room temperature.

3.3. Photocatalytic Activity in MB Decomposition

The photocatalytic activities of the PS@TiO$_2$ core–shell particles, the prepared TiO$_2$, the commercial P25, and the PS particles were evaluated using MB decomposition. Samples (10 mg) were added to 7 ppm aqueous MB solutions (100 mL). Thereafter, this suspension was stirred at 30 min in a black box (40 cm × 40 cm × 40 cm). Then, the photocatalytic reaction was started after irradiation with a UV lamp (365 nm) with the irradiation power (150 mW/cm^2) in the black box. A total of 3 mL of the mixture was withdrawn, and the pure aqueous MB solution was separated from the suspension by centrifugation at 3800 rpm for 5 min. The adsorption spectra of these solutions were recorded on spectrophotometer (UV-1800, Shimazu).

4. Conclusions

We synthesized PS@TiO$_2$ core–shell particles and demonstrated their photocatalytic activity in MB decomposition. In this method, TiO$_2$ nanoparticles prepared using the sol–gel method were collected on the surfaces of PS particles. Homogeneous PS@TiO$_2$ core–shell particles were obtained using 300 μL of an aqueous NH$_3$ solution and stirred at room temperature. TEM images showed that the TiO$_2$ shell thickness on the surfaces of the PS particles was approximately 5 nm. Additionally, Ti elements were confirmed to be present on the surfaces of the PS@TiO$_2$ core–shell particles using EDX analysis. The photocatalytic activities of the PS@TiO$_2$ core–shell particles were evaluated using MB decomposition. For comparison, we utilized TiO$_2$, prepared using the sol–gel method, and commercial P25. The MB decompositions of the PS@TiO$_2$ core–shell particles, the prepared TiO$_2$, and the commercial P25 after 24 min were 87%, 60%, and 58%, respectively. The crystallinity and shell thickness of TiO$_2$ on the surface of PS particles might play important role in MB decomposition. On the other hand, the reaction rates of the PS@TiO$_2$ core–shell particles between 0 and 4 min (21.3% min^{-1}) were faster than those of the commercial P25 (3.7% min^{-1}). Meanwhile, the rate of MB decomposition from 4 to 24 min was likely promoted in the presence of the PS@TiO$_2$ core–shell particles, probably because the surface of the PS@TiO$_2$ core–shell particles may have adsorbed the MB and its related decomposition products, leading to a decrease in photocatalytic activity. As one of the approaches to solve this problem, PS@TiO$_2$ core–shell particles can be synthesized via calcination to obtain TiO$_2$ hollow spheres.

References

1. Bastakoti, B.P.; Kuila, D.; Salomon, C.; Konarova, M.; Eguchi, M.; Na, J.; Yamauchi, Y. Metal–incorporated mesoporous oxides: Synthesis and applications. *J. Hazard. Mater.* **2021**, *401*, 123348. [CrossRef]
2. Olatidoye, O.; Thomas, D.; Bastakoti, B.P. Facile synthesis of a mesoporous TiO_2 film templated by a block copolymer for photocatalytic applications. *New J. Chem.* **2021**, *45*, 15761. [CrossRef]
3. Mahanta, U.; Khandelwal, M.; Deshpande, A.S. TiO_2@SiO_2 nanoparticles for methylene blue removal and photocatalytic degradation under natural sunlight and low–power UV light. *Appl. Sur. Sci.* **2022**, *576*, 151745. [CrossRef]
4. Priya, R.; Stanly, S.; Kavitharani, K.; Mohammad, F.; Sagadevan, S. Highly effective photocatalytic degradation of methylene blue using PrO_2–MgO nanocomposites under UV light. *Optik* **2020**, *206*, 164318.
5. Din, M.I.; Khalid, R.; Najeeb, J.; Hussain, Z. Fundamentals and photocatalysis of methylene blue dye using various nanocatalytic assemblies—A critical review. *J. Clean. Prod.* **2021**, *298*, 126567. [CrossRef]
6. Kumar, S.; Ahlawat, W.; Bhanjana, G.; Heydarifard, S.; Nazhad, M.M.; Dilbaghi, N. Nanotechnology–based water treatment strategies. *J. Nanosci. Nanotechnol.* **2014**, *14*, 1838–1858. [CrossRef] [PubMed]
7. Gaya, U.I.; Abdullah, A.H. Heterogeneous photocatalytic degradation of organic contaminants over titanium dioxide: A review of fundamentals, progress and problems. *J. Photochem. Photobiol. C Photochem. Rev.* **2008**, *9*, 1–12. [CrossRef]
8. Che Ramli, Z.A.; Asim, N.; Isahak, W.N.R.W.; Emdadi, Z.; Ahmad–Ludin, N.; Yarmo, M.A.; Sopian, K. Photocatalytic degradation of methylene blue under UV light irradiation on prepared carbonaceous TiO_2. *Sci. World J.* **2014**, *2014*, 13–15. [CrossRef]
9. Shen, R.; Hao, L.; Chen, Q.; Zheng, Q.; Zhang, P.; Li, X. P-Doped g-C_3N_4 Nanosheets with Highly Dispersed $Co_{0.2}Ni_{1.6}Fe_{0.2}P$Cocatalyst for Efficient Photocatalytic Hydrogen Evolution. *Acta Phys.-Chim. Sin.* **2022**, *38*, 2110014.
10. Lei, Z.; Ma, X.; Hu, X.; Fan, J.; Liu, E. Enhancement of photocatalytic H_2-evolution kinetics through the dual cocatalyst activity of Ni_2P-NiS-decorated g-C_3N_4 heterojunctions. *Acta Phys.-Chim. Sin.* **2022**, *38*, 2110049.
11. Lu, N.; Jing, X.; Xu, Y.; Lu, W.; Liu, K.; Zhang, Z. Effective cascade modulation of charge-carrier kinetics in the well-designed multi-component nanofiber system for highly-efficient photocatalytic hydrogen generation. *Acta Phys.-Chim. Sin.* **2023**, *39*, 2207045.
12. Lu, N.; Jing, X.; Zhang, J.; Zhang, P.; Qiao, Q.; Zhang, Z. Photo-assisted self-assembly synthesis of all 2D-layered heterojunction photocatalysts with long-range spatial separation of charge-carriers toward photocatalytic redox reactions. *Chem. Eng. J.* **2022**, *431*, 134001. [CrossRef]
13. Yan, X.; Wang, B.; Ji, M.; Jiang, Q.; Liu, G.; Liu, P.; Yin, S.; Li, H.; Xia, J. In-situ synthesis of CQDs/BiOBr material via mechanical ball milling with enhanced photocatalytic performances. *Chin. J. Struct. Chem.* **2022**, *41*, 2208044–2208051.
14. Hashimoto, K.; Irie, H.; Fujishima, A. TiO_2 Photocatalysis: A Historical Overview and Future Prospects. *Jpn. J. Appl. Phys.* **2005**, *44*, 8269. [CrossRef]
15. Bahnemann, D. Photocatalytic water treatment: Solar energy applications. *Sol. Energy* **2004**, *77*, 445–459. [CrossRef]
16. Ertuş, E.B.; Vakifahmetoglu, C.; Öztür, A. Enhanced methylene blue removal efficiency of TiO_2 embedded porous glass. *J. Eur. Ceram. Soc.* **2021**, *41*, 1530–1536. [CrossRef]
17. Legrand-Buscema, C.; Malibert, C.; Bach, S. Elaboration and characterization of thin films of TiO_2 prepared by sol–gel process. *Thin Solid Films* **2002**, *418*, 79–84. [CrossRef]
18. Lopez, T.; Sanchez, E.; Bosch, P.; Meas, Y.; Gomez, R. FTIR and UV-Vis (diffuse reflectance) spectroscopic characterization of TiO_2 sol-gel. *Mater. Chem. Phys.* **1992**, *32*, 141–152. [CrossRef]
19. Schneider, J.; Matsuoka, M.; Takeuchi, M.; Zhang, J.; Horiuchi, Y.; Anpo, M.; Bahneman, D.W. Understanding TiO_2 Photocatalysis: Mechanisms and Materials. *Chem. Rev.* **2014**, *114*, 9919–9986. [CrossRef] [PubMed]
20. Kasanen, J.; Salstela, J.; Suvanto, M.; Pakkanen, T.T. Photocatalytic degradation of methylene blue in water solution by multilayer TiO_2 coating on HDPE. *Appl. Sur. Sci.* **2011**, *258*, 1738–1743. [CrossRef]
21. Abd El-Rehim, H.A.; Hegazy, E.-S.A.; Diaa, D.A. Photo-catalytic degradation of Metanil Yellow dye using TiO_2 immobilized into polyvinyl alcohol/acrylic acid microgels prepared by ionizing radiation. *React. Funct. Polym.* **2012**, *72*, 823–831. [CrossRef]

22. Bertram, J.R.; Nee, M.J. A buoyant, microstructured polymer substrate for photocatalytic degradation applications. *Catalysis* **2018**, *10*, 482. [CrossRef]

23. Shigh, S.; Mahalingam, H.; Kumar Singh, P. Polymer-supported titanium dioxide photocatalysts for environmental remediation: A review. *Appl. Catal. A* **2013**, *462–463*, 178–195.

24. Mahshid, S.; Askari, M.; Sasani Ghamsari, M.; Afshar, M.; Lahuti, S. Mixed-phase TiO_2 nanoparticles preparation using sol–gel method. *J. Alloys Compd.* **2009**, *478*, 586–589. [CrossRef]

25. Luo, M.-L.; Tang, W.; Zhao, J.-Q.; Pu, C.-S. Hydrophilic modification of poly(ether sulfone) used TiO_2 nanoparticles by a sol–gel process. *J. Mater. Proc. Technol.* **2006**, *172*, 431–436. [CrossRef]

26. Wang, X.-J.; Li, F.-T.; Hao, Y.-J.; Liu, S.-J.; Yang, M.-L. TiO_2/SBA–15 composites prepared using H_2TiO_3 by hydrothermal method and its photocatalytic activity. *Mater. Lett.* **2013**, *99*, 38–41. [CrossRef]

27. Jiang, C.; Lee, K.Y.; Parlett, C.M.A.; Bayazit, M.K.; Lau, C.C.; Ruan, Q.; Moniz, S.J.A.; Lee, A.F.; Tang, J. Size–controlled TiO_2 nanoparticles on porous hosts for enhanced photocatalytic hydrogen production. *Appl. Catal. A* **2016**, *521*, 113–139. [CrossRef]

28. Wu, F.; Liu, W.; Qiu, J.; Li, J.; Zhou, W.; Fang, Y.; Zhang, S.; Li, X. Enhanced photocatalytic degradation and adsorption of methylene blue via TiO_2 nanocrystals supported on graphene–like bamboo charcoal. *Appl. Sur. Sci.* **2015**, *358*, 425–435. [CrossRef]

29. Deng, Z.; Chen, M.; Zhou, S.; You, B.; Wu, L. A Novel Method for the Fabrication of Monodisperse Hollow Silica Spheres. *Langmuir* **2006**, *22*, 6403–6407. [CrossRef]

30. Song, X.; Gao, L. Fabrication of Hollow Hybrid Microspheres Coated with Silica/Titania via Sol−Gel Process and Enhanced Photocatalytic Activities. *J. Phys. Chem. C* **2007**, *111*, 8180–8187. [CrossRef]

31. Leng, W.; Chen, M.; Zhou, S.; Wu, L. Capillary Force Induced Formation of Monodisperse Polystyrene/Silica Organic−Inorganic Hybrid Hollow Spheres. *Langmuir* **2010**, *26*, 14271–14275. [CrossRef]

32. Toyama, N.; Ohki, S.; Tansho, M.; Shimizu, T.; Umegaki, T.; Kojima, Y. Influence of alcohol solvents on morphology of hollow silica–alumina composite spheres and their activity for hydrolytic dehydrogenation of ammonia borane. *J. Sol-Gel Sci. Technol.* **2017**, *82*, 92–100. [CrossRef]

33. Rao, K.S.; El–Hami, K.; Kodaki, T.; Matsushige, K.; Makino, K. A novel method for synthesis of silica nanoparticles. *J. Colloid Inter. Sci.* **2005**, *289*, 125–131. [CrossRef]

34. Markowska–Szczupak, A.; Wang, K.; Rokicka, P.; Endo, M.; Wei, Z.; Ohtani, B.; Morawski, A.W.; Kowalska, E. The effect of anatase and rutile crystallites isolated from titania P25 photocatalyst on growth of selected mould fungi. *J. Photochem. Photobiol.* **2015**, *151*, 54–62. [CrossRef] [PubMed]

35. Zou, J.; Gao, J.; Xie, F. Anamorphous TiO_2 sol sensitized with H_2O_2 with the enhancement of photocatalytic activity. *J. Alloys Compd.* **2010**, *497*, 420–427. [CrossRef]

36. Wang, Z.; Zhang, F.; Yang, Y.; Xue, B.; Cui, J.; Guan, N. Facile Postsynthesis of Visible-Light-Sensitive Titanium Dioxide/Mesoporous SBA-15. *Chem. Mater.* **2007**, *19*, 3286–3293. [CrossRef]

37. Liaoa, M.-H.; Hsu, C.-H.; Chen, D.-H. Preparation and properties of amorphous titania-coated zinc oxide nanoparticles. *J. Solid State Chem.* **2006**, *179*, 2020–2026. [CrossRef]

38. Yang, J.-H.; Han, Y.-S.; Choy, J.-H. TiO_2 thin-films on polymer substrates and their photocatalytic activity. *Thin Solid Films* **2006**, *495*, 266–271. [CrossRef]

39. Metanawin, T.; Panutumrong, P.; Metanawin, S. Synthesis of polyurethane/TiO_2 hybrid with high encapsulation efficiency using one-step miniemulsion polymerization for methylene blue degradation and its antibacterial applications. *ChemistrySelect* **2023**, *8*, e202204522. [CrossRef]

40. Salehi Taleghani, M.; Salman Tabrizi, N.; Sangpour, P. Enhanced visible-light photocatalytic activity of titanium dioxide doped CNT-C aerogel. *Chem. Eng. Res. Design* **2022**, *179*, 162–174. [CrossRef]

41. Yang, Y.; Xu, L.; Wang, H.; Wang, W.; Zhang, L. TiO_2/graphene porous composite and its photocatalytic degradation of methylene blue. *Mater. Design* **2016**, *108*, 632–639. [CrossRef]

42. Li, X.; Lin, H.; Chen, X.; Niu, H.; Zhang, T.; Liu, J. Fabrication of TiO_2/porous carbon nanofibers with superior visible photocatalytic activity. *New J. Chem.* **2015**, *39*, 7863–7872. [CrossRef]

43. Kaur, K.; Singh, C.V. Amorphous TiO_2 as a photocatalyst for hydrogen production: A DFT study of structural and electronic properties. *Energy Procedia* **2012**, *29*, 291–299. [CrossRef]

44. Zhao, J.; Hidaka, H.; Takamura, A.; Pelizzetti, E.; Serpone, N. Photodegradation of surfactants. 11. zeta.–Potential measurements in the photocatalytic oxidation of surfactants in aqueous titania dispersions. *Langmuir* **1993**, *9*, 1646–1650. [CrossRef]

45. Imhof, A. Preparation and characterization of titania–coated polystyrene spheres and hollow titania shells. *Langmuir* **2001**, *17*, 3579–3585. [CrossRef]

46. Jang, I.B.; Sung, J.H.; Choi, H.J.; Chin, I. Synthesis and characterization of titania coated polystyrene core–shell spheres for electronic ink. *Synth. Met.* **2005**, *152*, 9–12. [CrossRef]

47. Toyama, N.; Umegaki, T.; Kojima, Y. Fabrication of hollow silica–alumina composite spheres and their activity for hydrolytic dehydrogenation of ammonia borane. *Int. J. Hydrogen Energy* **2014**, *39*, 17136–17143. [CrossRef]